Co-evolution ligands to Tecovirimat-resistant F13L mutations of MonkeyPox Virus

short title: monkeypox co-evolutionary docking

Coll, J*.
Department of Biotechnology. Centro Nacional INIA-CSIC. Madrid, Spain.
* Corresponding author
Email: juliocollm@gmail.com (JC)
Julio Coll, orcid: 0000-0001-8496-3493

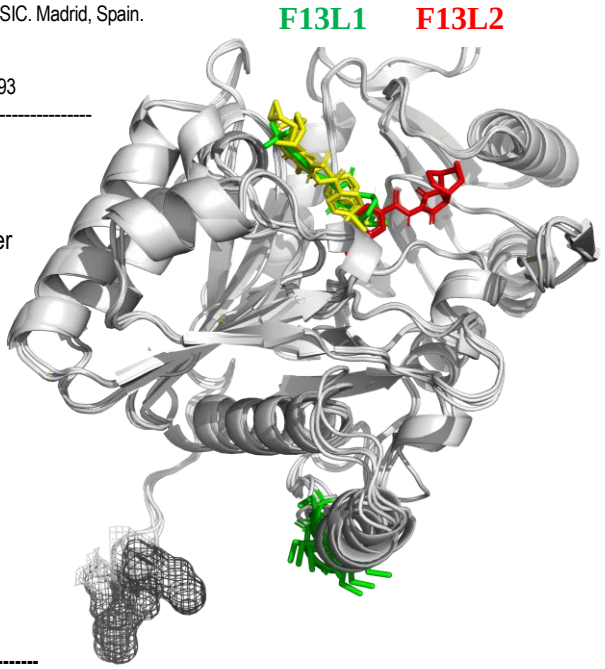

Abstract

Because of the emergence of F13L mutations in MonkeyPox Virus (MPXV)-infected patients with resistances to Tecovirimat-treatment, alternative drugs are actively searched. Aiming to help on these searches, computational strategies to generate rather than screen for new drug-like ligand candidates were explored here. Ligands were predicted by **i)** thousands of Tecovirimat-derived children generated by co-evolution fitting predicted docking cavities at either F13L1 or F13L2, and **ii)** docking Tecovirimat-derived top-children to F13L-mutant resistant models isolated from Tecovirimat-treated patients. Top-children-fitting F13L-mutant docking-cavities predicted novel scaffolds, nanoMolar affinities, high specificities, absence of known toxicities and similar conservation of their targeted Tecovirimat-docking cavities. Despite their limitations, similar proved-on-concept strategies might be fine-tuned to computational explore for new drugs docking to most prevalent Tecovirimat-resistance mutations.

Keywords: co-evolutionary docking; Tecovirimat-resistant mutations; ST-246; monkeypox virus; MPXV; MPOX; F13L

Introduction

This computational co-evolutionary work explored new ligand alternatives to Tecovirimat (ST-246 or TPOXX) maintaining docking to the Tecovirimat-resistant mutants that arised during the 2022 MPOX global outbreak of **M**onkey**P**o**x** **V**irus (MPXV) clade II and still to be identified in the 2024 clade I global outbreak. The Tecovirimat reference FDA-approved inhibitor for vaccinia poxvirus[2], was used here as the parent molecule to derive co-evolution children. Randomly generated children were selected by best fitting F13L alphafold modeled blind-docking identified cavities, including those from pooled mutations associated with Tecovirimat-resistance. Co-evolutions employed the ***D**ata**W**arrior **B**uild **E**volutionary **L**ibrary* (DWBEL) algorithms[2-5]. Briefly, DWBEL mimicked natural co-evolution by randomly generating tens of thousands of Tecovirimat-derived children, discarding those low fitting and saving the best F13L-fitted children[1], rather than screening preexisting large compound libraries. By incorporating Toxicity Risk assessment[1] and increasing computer memories during co-evolution, thousands of non-toxic children were generated that predicted drug-like properties, nanoMolar affinities, and higher specificities while conserving their initially targeted F13L mutant docking cavities.

The F13L (p37) are the most abundant of the poxviral membrane proteins[2]. Coding for 37 KDalton (372 amino acids)[3, 4], the F13L contains two residues that can be palmitoylated (^{185}CC), two phospholipase-like motifs (~ ^{121}xxxxDD and near-canonical ^{312}NxKxxxxD)[5-8], and one motif to interact with cellular TIP47 (^{253}YW) [9]. In vaccinia, F13L co-localizes [12, 27] with B5R (B6R orthologous in MPXV) [10-12], which could be also palmitoylated (^{301}C^{303}C)[13]. B5R(B6R) belong to transmembrane anchored glycoproteins of 42 KDalton (317 amino acids)[14] containing an extracellular domain, a transmembrane α-helix and a short cytoplasmic tail [15, 16]. F13L and B5R proteins are both required for vaccinia poxviruses to be released from their infected host-cells[17]. F13L and/or B5R deletions cause inhibition of membrane wrapping, fewer extracellular viral particles and attenuation of the resulting poxviruses[16,16-19].

As mentioned above, Tecovirimat was chosen here to target MPXV because it is a FDA-aproved inhibitor for vaccinia targeting F13L, active in vaccinia at low nanoMolar concentrations and which also inhibits MPXV infections[20-23, 29,18]. Thus, Tecovirimat and several analogues have been recommended to inhibit MPXV with an estimated EC_{50} of ~150 nM[19-22]. Tecovirimat is an small molecule containing a complex-ring structure, inhibiting poxviral membrane wrapping and replication of most poxviruses including vaccinia, MPXV, variola, smallpox, cowpox, camel, and others[23].. With respect to its mechanism of inhibition, it was demonstrated that Tecovirimat changes the intracellular membrane co-localizations of vaccinia F13L (from membrane to cytoplasm) and B5R (disaggregation from Golgi to vesicles)[24] and reduces the immunoprecipitation of F13L-B5R complexes[9]. However, despite its reported inhibitory activities, F13L-Tecovirimat complexes, nor F13L-B5R(B6R) structures have been crystallographically solved yet.

Surface shallow grooves were proposed as F13L-Tecovirimat docking cavities using different computational docking efforts[19, 25-27]. However, recent docking studies predicted internal MPXV amino acid residues for Tecovirimat contacts as its most probable binding site, validating their hypothetical interactions by molecular dynamic-docking studies [26] (**Table S3**, **yellow left**). Although the detailed mechanisms of inhibition are unknown, Tecovirimat has been proposed to conformationally disturb the F13L near-canonical phospholipase motif to interfere with its activity[26]. Alternatively, Tecovirimat may still fit other F13L binding cavities to block yet-unknown functions, include other allosteric influences on phospholipase activity or bind to possible F13L complexes with other proteins (i.e, poxviral B5R/B6R) to affect their subcellular location.

Tecovirimat-resistant mutations generated by *in vitro* cell culture identified targets at F13L amino acid residues conserved among several poxviruses[3, 4]. Some of those resistant mutations were located toward its carboxy-terminal domain[28, 29, 32]. Most recently, some of those earlier reported poxvirus mutations were confirmed while other were reported for the first time in MPXV patients resistant to Tecovirimat-treatment (**Table S2** and **Figure 1**[28-30]). These and other recent results suggested that in ~ 5 % of the MPXV patients, Tecovirimat resistant mutations arised during treatment, specially in immunocompromised patients where those percentages could be higher[31-33]. Preliminary use of Tecovirimat is beginning to be recommended for the most recent MPXV clade I global infections appearing during 2024 [34], despite some Tecovirimat-resistance most recently associated to advanced HIV patients suffering MPXV 2022 infections [35, 36]. Therefore, alternative drugs are needed, since despite many efforts[20], no other potent inhibitors targeting Tecovirimat-resistant poxviruses have been yet reported [28-30].

We report here some limited first attempts to generate large amounts of alternative ligands to Tecovirimat by DWBEL co-evolution in Alphafold modeled F13L pooled resistant mutants. The successful targeting of DWBEL to hypothetical Tecovirimat-resistant mutant cavities by co-evolution and blind-docking, required both high computer memories to apply toxicity risk assessments and specificity (molecular weight and hydrophobicity) to control their tendencies to increase during docking[6, 7, 8-11]. The accuracy of the predictions was improved by preserving 2D geometries to select for DWBEL consensus with **A**uto**D**ock**V**ina (ADV), recently identified as one of the most successful docking predictors[31].

The conservation of similar F13L-Tecovirimat predicted docking cavities in the top-children ligands to the F13L resistant mutants, could be interpreted as a favorable prediction sign of their possible MPXV inhibitory activities. However, predictions remain highly hypothetical because the absence of crystallographic structures, limitation to pooling the most abundant resistant mutations and/or lack of experimental confirmations. Nevertheless, perhaps similar strategies could be applied once the prevalence of 2024 outbreak Tecovirimat-resistant MPXV mutants would be more studied.

Further explorations using the most recent DWBEL version 6 using Liberica Java which improves the handling of memories during co-evolution may allow new penetration into the vast drug-space of Tecovirimat alternatives.

Computational Methods

Modeling of F13L from the MPXV 2022 strain with Tecovirimat-resistant mutations

The amino acid sequences corresponding to the F13L from the 2022 multinational outbreak of MPXV infection corresponding to isolate clade IIb lineage B.1 (containing the E353K mutation)[23], was downloaded from GenBank URK20480. The F13L amino acid sequence was alphafold modeled (F13L0) (https://colab.research.google.com/github/sokrypton/ColabFold/blob/main/AlphaFold2.ipynb), obtaining a **R**oot **M**ean **S**quare **D**eviation (RMSD) of 9.6 Å with the crystallographic model of phospholipase D of *Streptomyces sp* (ID 1v0y) at https://www.rcsb.org/structure/)[5].

The F13L coding for pools of the most abundant Tecovirimat-resistant mutations[23] (**Table S2 and Figure 1 red solid circles**) were introduced into their amino acid sequences before being uploaded to Alphafold. The five alphafold models obtained in each case predicted minimal RMSD of ~ 0.2 Å differences among them. Therefore, the corresponding number 1 models were selected for the computational studies. The new mutants contained a pool of the common *E353K* and the most abundant Tecovirimat-resistant mutations as follows, mutant **F13L1** (mutations *E353K*+N267D+ A288P+ A290V+ D294V+ A295E+ I372N) and mutant **F13L2** (mutations *E353K*+ N267deleted+ A288P+ A290V+ D294V+ A295E+ I372N). The **F13L2** alphafold model required one additional "clean geometry" step by Discovery Studio, to relax their predicted 3D structure as required for DWBEL, most probably due to the inclusion of the N267 deletion.

The PubChem (https://pubmed.ncbi.nlm.nih.gov/) 2D and 3D sdf files of Tecovirimat (ST-246 or TPOXX) 4-trifluoromethyl-N-(3,3a,4,4a,5,5a,6,6a-octahydro-1,3-dioxo-4,6-ethenocycloprop[f] isoindol-2(1H)-yl)-benzamide [23] and Ciclofovir, IMCBH (Nisonicotinoyl-N,-3-methyl-4-chlorobenzoylhydrazinc)[37], were employed as F13L poxviral high- and low-binding reference ligands, respectively.

The DataWarrior "Build Evolutionary Library"

The DataWarrior (DW) program written in java and updated was downloaded (https://openmolecules.org/datawarrior/download.html) following the details for the Windows version (dw550win.zip for Windows), as described before [1, 38].

The DW/Chemistry/Build Evolutionary Library (DWBEL) was loaded with the corresponding *.pdb ADV blind-docking docked files to provide the target docking cavities and with *.sdf files to provide the 2D structure of Tecovirimat. Preference criteria values and their weights for DWBEL co-evolution were as follows: minimal DW docking-scores (weight 4), molecular weight <= 600 g/mol, LogP <= 4 (weight 1) and Toxicity Risks <=1 (weight 4).

To best preserve 2D geometries of the generated children, the DW mmff94s+ force-field minimization algorithm[39] was critical[38]. DW docking ranked the children by unit-less relative negative values (the more negative, the higher affinities). From each parent, 3 consecutive runs generated thousands of unique best-fitting children molecules[1]. The raw children *.dwar files permanently saved docking-scores, molecular weights, cLogP hydrophobicities, and cavity-children docked images. The *.dwar files labeled with their number of ligands and experiment name were filtered using a DW macro to exclude hundreds of children with remaining toxicities (Mutagenesis, Tumorigenicity, Reproductive interference, Irritant, and Nasty functions)[40].

To accurately prepare the children for external programs (i.e., PyMol, ADV docking), the following DW /File/Save Special/SD-File…. optimized options were selected to preserve 2D geometries of conformers when saving *.sdf files: Structure column: Docked Protonation State, SD-file version: Version 3, Atom coordinates: Docking pose, ☐option checked: checked Cavity & Natural Ligand, Compound name column: ID. These *.sdf files optimally uploaded to PyMol for visualization (using its split_states command[38]) and/or to PyRx/Obabel-ADV for minimization and *.pdbqt file generation for docking.

The AutoDockVina docking program

The **A**uto**D**ock**V**ina (ADV) program written in Python vs3.8 included into the PyRx-098/PyRx-1.0 package[46] (https://pyrx.sourceforge.io/), and home-modified to handle large number of ligands, was used as described before. As recently reported, ADV was the best binding predictor for 428 protein-ligand complexes (± 2 Å), among 9 other docking programs, including 2 new amino acid sequence-smile-only algorithms, with the highest 52.3 % of success prediction rate[41]. ADV was employed here to explore alternative docking cavities than those identified by *DW*, to compare ADV affinities with *DW* docking-scores, to estimate relative docking in ~nanoMolar (nM) affinities and to generate detailed PyMol protein / children 3D images[38, 42-44]. Briefly, Obabel minimization and *.pdbqt file conversion of F13L proteins and children ligands[45] were generated by employing the mmff94s (Merck) force-field (most similar to the DWBEL mmff94s+). Children ligands were supplied to Obabel-ADV as DWBEL generated *sdf files, saved as mentioned above to preserve their 2D geometries. Only one highest affinity conformer per child were analyzed in this work. Estimates of ADV ~ docking-scores in Kcal/mol[46, 43, 47, 48], were converted to ~ nM affinities by the formula, 10^{9}-(exp[Kcal/mol/0.592]). A blind-docking grid of 45x45x45 Å centered by PyMol / centerofmass, surrounding the whole F13L molecule models was employed.

Computational software and hardware

In this work, 128 Gb of computer RAM memory, and options for saving *.sdf file for optimal 2D conservation, were introduced compared to previous work. Details on **Table 1** were as described before[1] and included here for convenience, including the most recent Modular large chemical synthesis information.

Table 1
Software and hardware for computational manipulations

name	vs	Main use	url
DataWarrior (DW)	Updated 5.5.0 Windows/Linus	Evolutionary docking[34] Docking to protein cavity Mmff94s+ force-field 2D conservation *.sdf files NTN ToxicityNastic macro	https://openmolecules.org/ datawarrior/download.html) https://cheminfo.github.io/openchemlib-s/classes/ForceFieldMMFF94.html https://github.com/cheminfo/openchemlib-js/lob/e88e8a0/types.d.ts#L3334 https://openmolecules.org/forum/index.php?t=msg&th=662&start=0& https://openmolecules.org/forum/index.php?t=msg&th=632&start=0&
OBabel & AutoDockVina	Home-adapted PyRx 0.98/1.0	Force-field minimization & 2D-reliable docking	https://pyrx.sourceforge.io/
MolSoft	3.9 Win64bit	Manipulation of *.sdf files	https://www.molsoft.com/download.html
PyMol 2023	2.5.7.	Visualization of molecules 3D alignment	https://www.pymol.org/
Discovery Studio	21.1.1.0.20298	Visualization of molecules Structure/clean geometry	https://discover.3ds.com/discovery-studio-visualizer-download
OriginPro	2022	Mathematical, statistical calculations and Figures	https://www.originlab.com/
LigPlus+	2.2.8.	Amino acid targeted by docked ligands around 4 Å	https://www.ebi.ac.uk/thornton--rv/software/LigPlus/applicence.html
Modular large chemical synthesis	2024	Commercially available modular chemical synthesis and analogues	Enamine https://enamine.net Enamine Real Space https://enamine.net/compound-collections/real-compounds Freedom Space 3.0 https://chem-space.com/compounds/freedom-space ChemSpace http://chem-space.com/search AlipheronHyperspace https://www.alipheron.com/products/hyperspace_dw_plugin/
AMD Ryzen i9 computer	4 DDR4 x 32 Gb memory	47 CPU Computational hardware	https://www.pcspecialist.es/

Results

F13L mutant models

Early for a complete scenario of MPXV Tecovirimat-resistance individual mutations and multi-mutations (mutants), representative studies of the 2022 outbreak mapped the most important F13L amino acid mutations emerging on Tecovirimat-treated 26 patients[23,29,30] (**Figure 1, Table S2**). This previous work may constitute the largest number and best characterized Tecovirimat-resistant MPXV isolates from humans reported to date [23,29,30]. All those 2022 MPXV isolates belonged to the clade IIb lineage B.1, which codes for the F13L *E353K* mutation (unrelated to Tecovirimat resistance), compared to the reference MPXV strain isolated in 2003[23] or with the still partially characterized clade I of the most recent 2024 outbreak[34]. Together with other sources of possible Tecovirimat-resistant mutations and because it is not yet clear which of the individual- or multi-mutation mutant isolates could be the main responsible of the Tecovirimat-resistance or alternatively be required for poxviral survival, the models studied here included the most abundant mutations reported from several sources (**Figure 1**, **green** and **red** circles), including: **i)** earliest reported poxvirus F13L mutations generated by *in vitro* selection[26], **ii**) mutations found at F13L by screening healthy patients[23,29,30] and **iii)** mutations isolated from Tecovirimat- treated patients[23,29,30] (**Table S2**). Most of the Tecovirimat-resistant mutations mapped between F13L ~ 200 to 300 amino acid residues, before the near-canonical phospholipase-like motif (**Figure 1, green** and **red** circles). In contrast, both *E353K* (unrelated to Tecovirimat-resistance) and I372N, mapped after the phospholipase motif. The phospholipase gap of mutations (**Figure 1 yellow vertical line**), could be explained for the need to preserve phospholipase activity for poxviral survival and/or replication.

Among all single F13L mutations, those showing Tecovirimat-resistance phenotypes with the highest EC_{50} > 500 µM were included into several mutants designed here (**Figure 1, red solid spheres**). These high EC_{50} mutants suggest that several single mutations might be necessary to confer the highest Tecovirimat-resistances. Compared to the MPXV reference strain clade IIa (2003) with a susceptibility of EC_{50} = 17.5 nM Tecovirimat (published data from Table 2 of Smith et al[23,29,30]), the resistant mutations showing higher EC_{50}, suggested to the authors of those studies that they were Tecovirimat-treatment-dependent, specially those emerging from immuno-compromised patients.

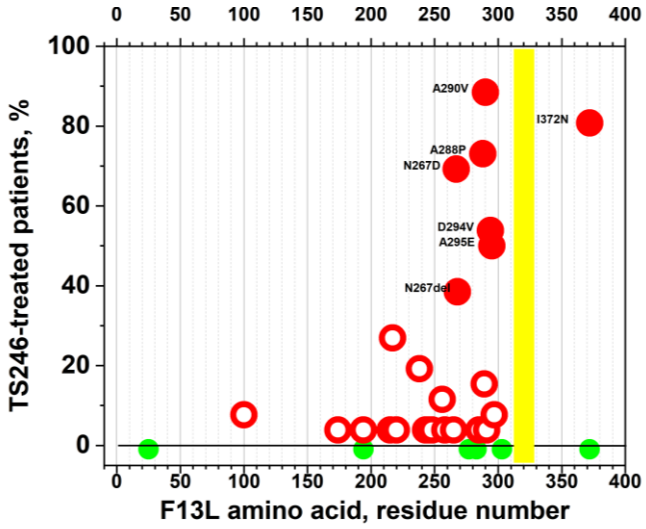

Figure 1
Single amino acid mutations in F13L implicated in Tecovirimat-resistance
Single mutations from single- or multi-mutant isolates were counted in 26 patient isolates (**Table S2**)[23]. Their percentages were calculated by the formula, 100 * number of single mutations / 26 (data from Table 2[30]). All the MPXV 26 isolates from the 2022 outbreak at Los Angeles USA coded for *E353* [23,29,30]. The A290V and A288P mutations were isolated in persistent MPXV infections despite Tecovirimat treatments [49, 50]. Single amino acid mutations were labeled to their left (wild-type amino acid+position number+mutation).
Yellow vertical rectangle, mapped nearby-canonical phospholipase-like motif ([312]NxKxxxxD)[5, 6]
Green solid circles, mutations isolated *in vitro* by cell co-culture of several poxviruses with Tecovirimat[26].
Red circles, single mutations identified from 26 patient isolates assayed for Tecovirimat-resistance.

To explore for possible new ligands to F13L-mutants by DWBEL co-evolution, the most abundant representative F13L mutants were included into the amino acid F13L sequence before being Alphafold modelled. The 2003 MPXV reference strain (F13L-1), the *E353K* clade IIb mutation of the 2022 outbreak (F13L0) and the representative pooled mutants coding for the most abundant and highest EC_{50} Tecovirimat-resistant mutations (**F13L1** and **F13L2**) were all Alphafold modelled (**Figure 1, labelled red solid circles**).

Because the main objective of this work was to test prove-of-concept computational strategies rather than to develop a practical application, a minimal

number of two representative F13L mutant models containing the most abundant and higher Tecovirimat-resistant mutations were selected for these preliminary studies (**Figure 1, mutation labelled red solid circles**). Two models were minimally required because the N267D / N267deleted mutations exclude each other. None of them should be discarded due to their high frequencies and the high F13L structural impact the N267 deletion may have. In addition to the single mutations, the common 2022 background mutation *E353K* was also included. Therefore, the artificially designed pooled-mutant models were, **F13L1** (coding for *E353K* + N267D + A288P + A290V + D294V + A295E + I372N) and **F13L2** (coding for *E353K* + N267deleted + A288P + A290V + D294V + A295E + I372N).

ADV blind-docking of Tecovirimat to F13L-1, F13L0, F13L1 and F13L2

For ADV blind-docking, a PyMol centered 45x45x45 Å grid (similar to the one proposed for the F13L MPXV strain isolated in 2007[27]), was selected after evaluating different grids **(Table S1)**.

Results from the ADV blind-dockings predicted similar Tecovirimat docked cavities for F13L-1, F13L0 and **F13L1** (**Figure 2, yellow and green** sticks), while a nearby, but different, cavity was Tecovirimat-docked to **F13L2** (**Figure 2, red sticks**). Tecovirimat-docking to **F13L2** appears to be more affected than any of the other F13L models most probably because of its N267 deletion.

Tecovirimat-docking to F13L0, predicted similar amino acids at 4 Å distance than those reported before[27] (**Table S3, yellow left columns**). The wide blind-docking grid, allowed the exploration of any alternative docking cavities, while predicted the highest affinities for Tecovirimat and IMCBH[51] **(Table S1)**. The near canonical phospholipase-like motif (^{312}NxKxxxxD)[5, 6], their probable ^{334}H ^{338}H requirements for phospholipase activity, and the *E353K* mutation present in all isolates of the MPXV 2022 outbreak, mapped behind the docked Tecovirimat (**Figure 1**, **Blue background ellipse, and Table S3, yellow columns**).

Figure 2
Tecovirimat-docked to F13L models
Tecovirimat was ADV blind-docked to F13L-1 (reference 2003 strain), F13L0 (common *E353K* mutation of the 2022 clade IIb), and Tecovirimat-resistant **F13L1** and **F13L2** 2022 mutants. The individual F13L images were merged in PyMol.
Gray cartoons, merged F13L-1, F13L0, **F13L1** and **F13L2** amino acid carbon alpha backbones.
Yellow sticks, Tecovirimat-docked to F13L-1 and to F13L0.
Green sticks, Tecovirimat-docked to **F13L1**.
Red sticks, Tecovirimat-docked to **F13L2**.
Green sticks down, palmytoil sites at ^{185}CC
Black mesh down, amino terminal ^{1}Met
Blue background ellipse, ~ nearby-canonical phospholipase-like ^{312}NxKxxxxD motif and required ^{334}H^{338}H, mapping behind the Tecovirimat-docked cavities.

DWBEL-derived top-children fitting F13L1 and F13L2 mutants

Because DWBEL co-evolutions from the whole Tecovirimat molecule predicted co-evolved children with higher affinities and lower toxicities than Tecovirimat molecular fragments (data not shown), whole Tecovirimat was chosen as the DWBEL-parent for further work. Because targeting several molecular weight children preferences, such as <280, <300, <400, <500 or <550 g/mol, did not greatly increased their affinities (**Figure S1, up**), molecular weights < 600 g/mol were used as co-evolution criteria. Molecular weights > 600 g/mol were discarded because of the risk to increase both unespecificity and computer memory demands. The computer memories were increased from 60 to 120 Gb to best target children < 600 g/mol, to avoid program crashes, to improve co-evolution speed and to increase the number of non-toxic fitted-children (**Figure S1, up**). Such high computer memories may be required for the DWBEL program to keep track of the randomly generated tens of thousands of raw children and to select thousands of unique fitted-children[1]. The progressive reduction of docking-scores, visualized the increased children affinities selected during each of three consecutive co-evolution runs at different targeted molecular weights (**Figure S1, down**).

Most of the **F13L1** (**green**) and **F13L2** (**red**) children from DWBEL and ADV predicted higher affinities than the initial Tecovirimat-parent (**Figure 3 green** and **red solid circles,** respectively). However, because of their very different algorithms for calculations and targeted cavity/grid identifications, the DWBEL docking-scores did not exactly correlated with ADV affinities (**Figure 3, green** and **red**).

To select those top-children predicting the highest affinities in both DWBEL and ADV, consensus affinities were selected using a home-made Python script (**Supplementary Materials / DWBELvsADVconsensus.py).**

For the **F13L1** consensus, top-children were selected predicting both DWBEL docking-scores < - 85 and ADV affinities < -11 kcal/mol to yield 32 top-children consensus. Representative 32 top-children targeted similar **F13L1** docking-cavities (**Figure 4, F13L1**) than Tecovirimat in **F13L1** (**Figure 2, green**). These representative top-children consisted in two different scaffolds of 6 rings with different atom extensions, 2-3 Nitrogen atoms and 6 Oxygen atoms (examples at **Figure 5, F13L1: 12326** and **8181,** and **Table 2**).

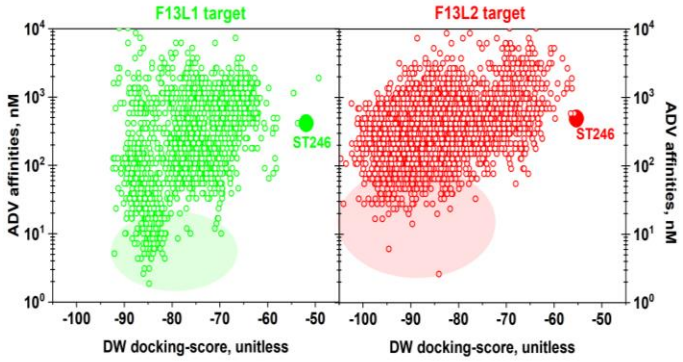

Figure 3
ADV *versus* DWBEL of Tecovirimat-derived children targeting F13L1 or F13L2
The corresponding **F13L1**- or **F13L2**-Tecovirimat docked cavities were targeted by DWBEL to generate children from the Tecovirimat-parent. Then, the DWBEL children were blind-docked by ADV using a 45x45x45 Å grid to identify possible alternative cavities and quantify their affinities in ~ nM. Complete data corresponding to these Figures were included at **Supplementary Materials / 1769F13L1.sdf and 3537F13L2.sdf**.
Green open circles, **F13L1**. **Solid green circle**, Tecovirimat (ST246). **Green oval background**, **F13L1** top-children.
Red open circles, **F13L2**. **Solid red circle**, Tecovirimat (ST246). **Red oval background**, **F13L2** top-children.

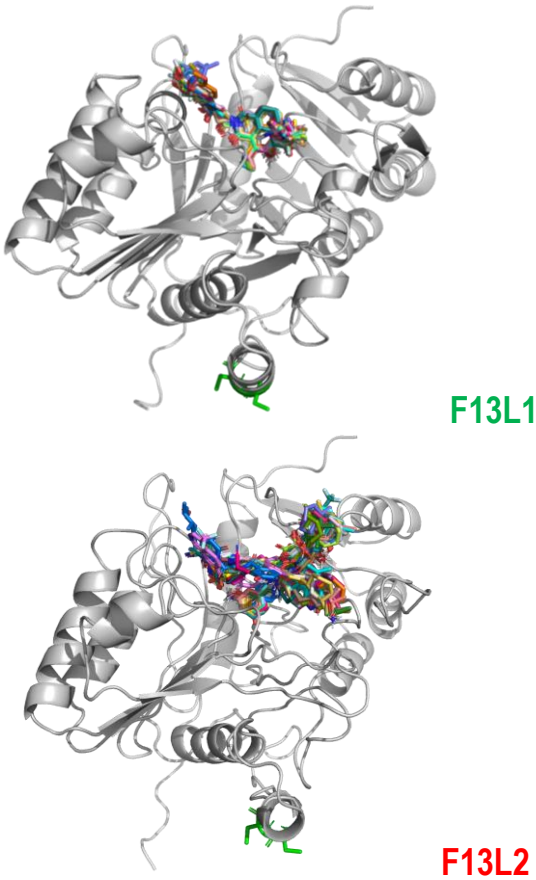

Figure 4
Mapping of top-children derived from Tecovirimat targeting F13L1 and F13L2 docking-cavities
Gray cartoons, carbon backbone of **F13L1** and **F13L2** as in **Figure 2**.
Green sticks in F13L α-helix Dipalmitoylated 185 and 186 Cysteines of F13L
Multicolor sticks, 32 or 36 top-children docked to **F13L1** or **F13L2**, respectively.

For the **F13L2** consensus**,** top-children were selected predicting both DWBEL docking-scores < - 90 and ADV affinities < -10 kcal/mol (as described above) to yield 36 top-children consensus. Some of the representative 36 top-children targeted similar **F13L2** docking-cavities (**Figure 4, F13L2**) than Tecovirimat in **F13L2** (**Figure 2, red**), while other targeted similar docking-cavities than those targeted by Tecovirimat in **F13L1** (**Figure 2, green**). Representative top-children consisted in 3 branches extended from a central carbon with two different scaffolds of different atom extensions, 3 Nitrogen atoms and 6-7 Oxygens (examples at **Figure 5, F13L2: 35702** and **34853,** and **Table 2**).

Molecular weights, LogP hydrophobicities, DWBEL docking scores, ADV nM affinities and docked conformers of **F13L1** or **F13L2** consensus top-children were supplied (**Supplementary Materials / 32F13L1.sdf, 36F13L2.sdf, 32F13L1.pse** and **36F13L2.pse**).

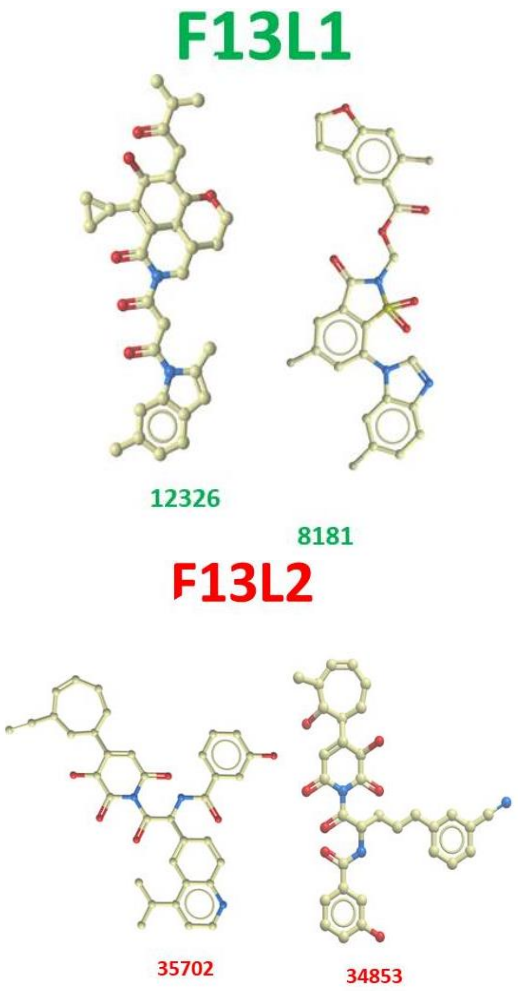

Figure 5
2D structures of representative scaffolds of DWBEL+ADV consensus F13L1 or F13L2 top-children
2D structures were drawn with MolSoft. **Red spheres**, Oxygens. **Blue spheres**, Nitrogens. **Light green spheres/sticks**, Carbons and their bonds. Complete consensus **F13L1** and **F13L2** top-children data were provided at **Supplementary Materials / 32F13L1.sdf, 36F13L2.sdf, 32F13L1.pse** and **36F13L2.pse**

Table 2
Properties of representative scaffolds of DWBEL+ADV top-children

Target: Children	DWBEL score, unitless	ADV, nM	Target sites	MW, g/mol	logP	Chemical formula
F13L1:						
12326	-84.8	1.8	X	546	3.5	C32H38N2O6
8181	-81.5	4.3	X	527	4.0	C24H16F3N3O6S
F13L2:						
35702	-94.6	6.0		591	3.5	C35H35N3O6
34853	-95.6	16.7	X	571	2.8	C32H33N3O7

X targeted sites, F13L1-Tecovirimat docking cavity (**Figure 2, yellow green sticks**). **Unlabelled targeted sites, F13L2**-Tecovirimat docking cavity (**Figure 2, red sticks**)

The identification of the **F13L1** and **F13L2** amino acids surrounding their docked complexes with the DWBEL+ADV consensus top-children, confirmed the visualized differences among the representative top-children scaffolds (**Table S3**). Previously unreported, the docking to the **F13L1** and **F13L2** mutants containing the pooled mutations isolated from Tecovirimat-resistant patients, identified some new possible targeted amino acids, compared to previous studies. Nevertheless, there were many coincidences with some of the amino acids previously reported to be targeted by Tecovirimat docked to the MPXV F13L isolated in 2007 [27]. For instance, the new top-children targeted amino acids ^{312}N, and ^{334}H ^{338}H located at the near canonical phospholipase-like motif and their Histidine putative requirements, some of them predicting Hydrogen bonds (**Table S3, red H**). Additionally, one of the top-children (35702), predicted Hydrogen bonds to ^{283}D, one of the amino acids mutated in resistant MPXV and previously isolated by *in vitro* resistance to both Tecovirimat and IMCBH [26].

Discussion

In this preliminary work, Alphafold-predicted F13L coding for artificially-constructed mutants by pooling some of the most abundant mutations were targeted to offer a simplified prove-of-concept application of DWBEL co-evolutions. The initial attempts to co-evolve Tecovirimat-derived ligands were unsuccessful due to the shallow grooves targeted at previously proposed F13L docking surface targets. Apparently, such targets were not capable to generate appropriated cavities for high affinity docking even when increasing computer memories and the number of co-evolution runs. After numerous trial-and-error efforts, an alternative strategy was successfully developed, consisting in: **i)** Including both highly specific non-toxic filtering during co-evolution together with higher computer memories, **ii)** Improving 2D structure conservation during the data exchanges between DWBEL / ADV programs by using mmff94s**+** force-field conformers (six alternative force-fields altered 2D structures and affinities), and **iii)** Exploring alternative F13L inner cavities as detected by blind-docking.

Pending on solved crystallographic F13L structures, several docking cavities were identified as possible F13L new docking targeting candidates by blind-docking. Furthermore, to complicate F13L docking interpretations, different binding cavities may co-exist or be exchanged by mutations during one MPXV human outbreak, even within the same patient. Because of these docking-cavity uncertainties, we also explored some of most recent machine-learning new algorithms using transformers[78, 91,52-54] relying only on protein amino acid sequence rather than docking cavities[55, 56]. Among all those that were tested, the **H**ighlights **o**n **T**arget **S**equences (HoTS), was the most reproducible and successful method to predict docking cavities[91] when applied to F13L (data not shown). Trained with only 232 protein-ligand known complexes, HoTS claimed a successful prediction of ~ 66 % binding cavities from not-seen-before protein sequences[91,57], despite the protein-ligand pair limitations for model training[58]. In our hands, HoTS predicted some of the F13L docking-cavities described before and here (data not shown). However, HoTS was slow when compared to the speed at which thousands / hundreds of ligand children were generated by DWBEL. It appears that sequence-only docking methods would still require more development efforts [58, 59].

Many of the amino acids predicting Tecovirimat[27] docking contacts were confirmed in the consensus top-children, including those amino acids surrounding the canonical phospholipase-like motif and their nearby ^{334}H,^{338}H[5], suggesting new unexplored cavities as possible future targets.

The consensus top-children predictions proposed here are limited in their possible drug-like applications because: **i)** the small number of available mutations characterized from Tecovirimat-resistant patients, **ii)** the mutant strategy of pooling the most abundant mutations, rather than targeting one-by-one each individual mutations, and **iii)** the absence of F13L crystallographically solved models. Apart from all those mentioned above, other limitations arised, for instance, because the fixed rather than dynamic docking-cavities employed, the absence of water interactions, or the always incomplete exploration of the vast chemotype/chemical space alternatives[38, 39]. Additionally, most probably other docking cavities still remain to be further explored, such as those that may be appearing at the interfaces of F13L with other interacting proteins like B6R-poxvirus, and/or TIP47-host proteins. Nevertheless, the proposed strategy might be valid to raise more ligands for future work when more F13L mutations would be available. The MPXV 2022 global outbreak identifying F13L mutations appearing on Tecovirimat-resistant immuno compromised human patients, suggests that alternative Tecovirimat drugs are required to include those from the most recent 2024 outbreak[33]. Some of these ideas may help to explore alternative ligands by using the most recent DWBELvs6 written in more recent Java (BellSoft Liberica openJDK, https://bell-sw.com/liberica) which allowed for optimal use of computer memories during DWBEL co-evolutions (https://openmolecules.org/forum/index.php?t=msg&th=748&start=0&).

Some of the most remarkable results on MPXV F13L mutants were the high speed to generate high numbers of unique nanoMolar affinities fitting the **F13L1** and **F13L2** mutant model cavities. Many different co-evolution trajectories were identified when providing higher computer memories and more consecutive runs. However, chemical synthesis will be required for confirmatory experimental tests. At this time some recent breakthrough ultrasearch technologies targeting extralarge combinatorial chemical spaces are becoming available from several companies. Among them, Enamine (https://enamine.net), Enamine Real Space (https://enamine.net/compound-collections/real-compounds), Freedom Space 3.0 (https://chem-space.com/ compounds/freedom-space), and ChemSpace (http://chem-space.com/search). For instance, the Alipheron Hyperspace, available from the new DW 6.2 version (https://www.alipheron.com/products/hyperspace_dw_plugin/), offers > ~ 50000 millions of virtual molecules by cheap-fast combinatorial chemical synthesis. Some of these novel modular combinatorial synthesis methodologies may allow to experimentally test a high number of computational predictions with lower synthesis costs.

Supporting Information

Table S1
Tecovirimat (ST246) and IMCBH binding and preliminary docking to F13L

method	pox target	F13L model	Grid center, Å X	Y	Z	Grid size, Å	Tecovirimat (ST246) ~ nM	IMCBH ~ nM	reference
EC50	VACV	Binding	-----	-----	-----	----------	6	65000	[51]
QVina	MPXV	afold*	?	?	?	?	820	?	[25]
DiscoveryStudio	MPXV	afold**	-6.2	-2.4	-8.6	8.9 sphere	15	?	[27]
ADV	MPXV	afold*	-6.2	-2.4	-8.6	8.9 sphere	820	?	[19]
ADV	VACV	afold**	-0.2	0.4	1.4	45x45x45	46	4400	selected
ADV	VACV	afold**	-0.2	0.4	1.4	60x60x60	50	1600	this work
ArgusLab	VACV	Swiss*	?	?	?	?	?	?	[26]
ArgusLab	VACV	afold*	-3.0	-3.0	0.9	25x25x25	6180	690	this work
ADV	VACV	afold*	-3.0	-3.0	0.9	25x25x25	6180	35600	this work

*, grid center defined by Tecovirimat (ST246)^r and IMCBH^r mutations. **, grid center automatically selected by LibDock (DiscoveryStudio) [27] or ADV[15] and this work.
EC_{50} , *in vitro* binding of Tecovirimat (ST246) and IMCBH[38] .
nM, affinities calculated from Kcal/mol of ADV docking-scores by the formula, nM = 10^9-(exp(Kcalmol/0.592)).
Qvina, QuickVina.
ADV, AutoDockVina.
VACV, **VAC**cinia **V**irus.
MPXV, **M**onkey**P**o**X** **V**irus.
Yellow background, grids selected for this work

Table S2
F13L mutations in 26 patients treated with Tecovirimat (ST246) (data modified from Table 2 from Smith *et al* 2023[30])

Mutations	Isolation	Number isolates	Reference
F25V	CMLV	-	[26]
D100N	patients	2	[30]
K174N	patient	1	[30]
H194N	patient+MPXV	1	[26, 30]
S215F	patient	1	[30]
D217N	patients	7	[30]
T220A	recent	?	[29]
H238Q	patients	5	[29, 30]
P243S	patient	1	[29, 30]
T245I	patient	1	[29, 30]
D248N	patient	1	[30]
D256N	patients	3	[30]
Y258C	patient	1	[30]
A265D	recent	-	[29]
N267D	patients	18	[20, 29, 30]
N267deleted	patients	10	[20, 29, 30]
G277C	VACV,CMLV,MPXV	-	[26, 51]
D283Y	patient +MPXV	1	[26, 30]
I285H	patient	1	[30]
A288P	patients	19	[29, 30]
T289A	patients	4	[29, 30]
A290V	patients+VACV patient	23	[20, 29, 30]
R291K	patient	1	[30]
D294V	patients	14	[29, 30]
A295E	patients	13	[30]
L297inserted	patients	2	[30]
D301deleted	patient	?	[30]
S369L	patient	?	[30]
SVK303-305	MPXV	-	[26]
E353K	2022 outbreak	26	[30]
I372N	patient +VACV,CMLV	21	[26, 29, 30]

Blue background Tecovirimat-resistant mutations from either patients or *in vitro*
Light blue background, recently detected, not yet assayed for Tecovirimat resistance
Strong blue background, The 26 MPXV isolates belonged to clade IIb lineage B.1 coding for the E353K mutation compared to the previous reference strain.
Reddish background, most abundant mutations mapped alone or together

VACV, *in vitro* isolated **VAC**cinia **V**irus resistance mutations
MPXV, *in vitro* isolated **M**onkey**P**o**X** **V**irus resistance mutations
CMLV, *in vitro* isolated **C**a**M**e**L** **V**irus resistance mutations

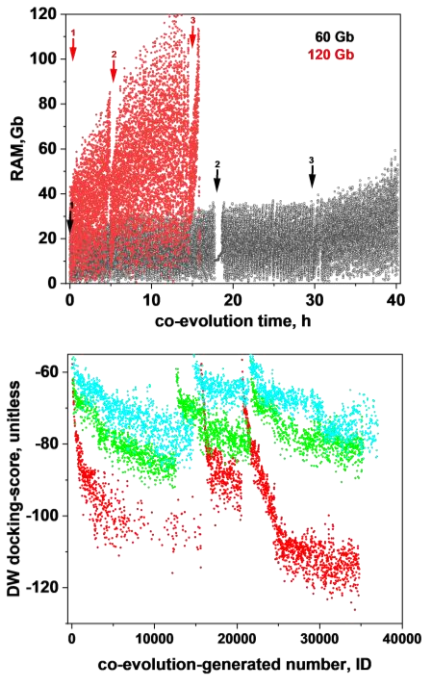

Figure S1
Memory timing during DWBEL co-evolutions using 60 or 120 Gb memories (UP). Children docking-scores *vs* their co-evolution-generated ID numbers at different molecular weights (DOWN)
The DWBEL co-evolution randomly generated raw children molecules from their Tecovirimat-parent molecule with consecutive ID numbers, keeping all data in memory to avoid repetitions. Each consecutive runs randomly re-starts the initial Tecovirimat-parent for a unique new co-evolution pathway. **Blue**, targeting children < 300 g/mol. **Green**, targeting children < 400 g/mol. **Red**, targeting children < 600 g/mol.

Table S3
F13L-1, F13L0. F13L1 and F13L2 amino acids nearby 4 Å of ADV docked top-children

F13L residue position		Amino acids	F13L0-Tecovirimat	F13L1-Tecovirimat	12326	8181	F13L2-Tecovirimat	35702	34853
52	F	Phe							
53	C	Cys							
55	N	Asn		H		H			
58	S	Ser		H					
86	A	Ala							
89	R	Arg							
116	L	Leu							
118	L	Leu							
120	C	Cys							
133	N	Asn						H	H
135	S	Ser		H	H			H	
137	T	Thr			H	H			
139	G	Gly							
140	S	Ser							
144	I	Ile							
239	L	Leu							
246	R	Arg						H	H
267	N	Asn					267▼		
279	W	Trp							
*280	D	Asp							
281	K	Lys	H			H			
282	N	Asn							
*283	D	Asp						H	
284									
311									
*312	N	Asn							H
*314	K	Lys	H						
326	S	Ser							
327	S	Ser			H				
328	N	Asn					H		
329	N	Asn						H	H
331	D	Asp							
333	T	Thr							
*334	H	His			H				H
*338	H	His						H	

Amino acid positions, were those at F13L0, except for the ^{267}N which was either mutated to D or deleted (▼ , **Purple** row). For comparative purposes, the identification numbers > 267 on the **F13L2** ^{267}N deleted mutations were corrected to their "initial" positions in F13L0 and **F13L1**.
***red number**, F13L amino acid at vaccinia mutation to both ST246 and IMCBH resistance[26] .
***green numbers**, F13L mapping of conserved amino acids at the near-canonical phospholipase-like motif in poxviruses and histidines possibly participating in their phospholipase activity.
Blue and yellow rectangle backgrounds, residues of **F13L1** and **F13L2** predicted nearby 4 Å to reference ligand and top-children atoms (LigPlus/LigPlot).
Yellow background numbers to the left, F13L amino acids previously identified by Tecovirimat (ST246) docking in the MPXV strain of 2007 (^{353}E) [27] .
H, LigPlus/LigPlot predicted Hydrogen bonds.

Supporting Materials

GraphycalAbstract.pse. Tecovirimat-docked to Alphafold modeled F13Ls **(**from **Figure 2).** Tecovirimat was ADV blind-docked to F13L-1 (2003 reference strain), F13L0 (*353K* mutation of the 2022 clade), and Tecovirimat-resistant pooled single mutations **F13L1** and **F13L2** coding for most abundant 2022 mutations. **Gray cartoons,** PyMol merged F13L-1, F13L0, **F13L1** and **F13L2** Alphafold modeled amino acid carbon alpha backbones. **Yellow sticks**, Tecovirimat-docked to F13L-1 and to F13L0. **Green sticks.** Tecovirimat-docked to **F13L1**. **Red sticks**, Tecovirimat-docked to **F13L2**. **Green sticks down**, F13L ^{185}CC palmytoil sites. **Black mesh**, F13L ^{1}Met amino terminal.

1769F13L1.sdf. Data from the 1769 Tecovirimat-derived non-toxic fitted-children (**Figure 3, F13L1**). The file contains conformer DWBEL generated order (ID), with their corresponding 3D chemical structures, molecular weights, cLogP hydrophobicities, unitless DWBEL docking-scores and kcal/mol ADV affinities. The file can be opened in freely-available either MolSoft (https://www.molsoft.com/download.html) or DW (https://openmolecules.org/datawarrior/download.htm).

3532F13L2.sdf. Data from the 3532 Tecovirimat-derived non-toxic fitted-children (**Figure 3, F13L2**). The file contains conformer DWBEL generated order (ID), with their corresponding 3D chemical structures, molecular weights, cLogP hydrophobicities, unitless DWBEL docking-scores and kcal/mol ADV affinities. The file can be opened in freely-available either MolSoft (https://www.molsoft.com/download.html) or DW (https://openmolecules.org/datawarrior/download.htm).

32F13L1.sdf. Data from 32 Tecovirimat-derived non-toxic fitted-top-children consensus of < -85 DWBEL and < -11 kcal/mol ADV (**Figure 3 F13L1** and **1769F13L1.sdf**). The file contains generated conformer DWBEL order (ID), with their corresponding 3D chemical structures, molecular weights, cLogP hydrophobicities, unitless DWBEL docking-scores and kcal/mol and nM ADV affinities. The file can be opened in freely-available either MolSoft (https://www.molsoft.com/download.html) or DW (https://openmolecules.org/datawarrior/download.htm).

36F13L2.sdf. Data from 36 Tecovirimat-derived non-toxic fitted-top-children consensus of < -90 DWBEL and < -10 kcal/mol ADV (**Figure 3 F13L2** and **3532F13L2.sdf**). The file contains generated conformer DWBEL order (ID), with their corresponding 3D chemical structures, molecular weights, cLogP hydrophobicities, unitless DWBEL docking-scores and kcal/mol and nM ADV affinities. The file can be opened in freely-available either MolSoft (https://www.molsoft.com/download.html) or DW (https://openmolecules.org/datawarrior/download.htm).

32F13L1.pse. 32 DWBEL+ADV consensus top-children conformers targeting **F13L1** (PyMol 2.5.3).

36F13L2.pse. 36 DWBEL+ADV consensus top-children conformers targeting **F13L2** (PyMol 2.5.3).

Funding
The work was carried out without any external financial contribution

Competing interests
The author declares no competing interests

Authors' contributions
JC designed, performed and analyzed the dockings and drafted the manuscript.

Acknowledgements
Thanks are due to Dra.M.Lorenzo and Dr.R.Blasco at CSIC-INIA Dpt.Biotecnologia Madrid (Spain) for their initial idea and critical reading of a previous version of this manuscript. Thanks are specially due to Dr. T.Sander, J.Wahl and N.Berndt of Idorsia Pharmaceuticals Ltd. at Allschwil (Switzerland) for their help with the Windows version of the Data Warrior Build Evolutionary Library, files to solve initial memory problems, and the inclusion of Toxicity risks assessment into the DWBEL algorithms. Special thanks to N.Berndt for his original discussions and help with the Toxicity - Nastic and 2D geometry conservation macro designs. Thanks are also due to Joshua Holliday of the PCSPECIALIST support team at Wakefield WF4 4TD England, for his help with the design and duplication of our computer RAM memories. Thanks also to Dr. A. Villena from the University of Leon (Spain) for maintaining a permanent flow of recent bibliography.

REFERENCES

[1]Coll, J.M. Exploring non-toxic co-evolutionary docking.*ChemRxiv.* 2023, https://chemrxiv.org/engage/chemrxiv/article-details/6512b162ade1178b2424c325: http://dx.doi.org/10.26434/chemrxiv-2023-rr5b0.

[2]Moss, B. Understanding the biology of monkeypox virus to prevent future outbreaks.*Nat Microbiol.* 2024, 9: 1408-1416 http://dx.doi.org/10.1038/s41564-024-01690-1.

[3]Husain, M. and Moss, B. Vaccinia virus F13L protein with a conserved phospholipase catalytic motif induces colocalization of the B5R envelope glycoprotein in post-Golgi vesicles.*J Virol.* 2001, 75: 7528-42 http://dx.doi.org/10.1128/JVI.75.16.7528-7542.2001.

[4]Husain, M., *et al.* Topology of epitope-tagged F13L protein, a major membrane component of extracellular vaccinia virions.*Virology.* 2003, 308: 233-42 http://dx.doi.org/10.1016/s0042-6822(03)00063-1.

[5]Leiros, I., *et al.* The reaction mechanism of phospholipase D from Streptomyces sp. strain PMF. Snapshots along the reaction pathway reveal a pentacoordinate reaction intermediate and an unexpected final product.*J Mol Biol.* 2004, 339: 805-20 http://dx.doi.org/10.1016/j.jmb.2004.04.003.

[6]Bryk, P., *et al.* Vaccinia Virus Phospholipase Protein F13 Promotes Rapid Entry of Extracellular Virions into Cells.*J Virol.* 2018, 92: http://dx.doi.org/10.1128/JVI.02154-17.

[7]Koonin, E.V. A duplicated catalytic motif in a new superfamily of phosphohydrolases and phospholipid synthases that includes poxvirus envelope proteins.*Trends Biochem Sci.* 1996, 21: 242-3 http://dx.doi.org/S0968-0004(96)30024-8 [pii].

[8]Ponting, C.P. and Kerr, I.D. A novel family of phospholipase D homologues that includes phospholipid synthases and putative endonucleases: identification of duplicated repeats and potential active site residues.*Protein Sci.* 1996, 5: 914-22 http://dx.doi.org/10.1002/pro.5560050513.

[9]Chen, Y., *et al.* Vaccinia virus p37 interacts with host proteins associated with LE-derived transport vesicle biogenesis.*Virol J.* 2009, 6: 44 http://dx.doi.org/10.1186/1743-422X-6-44.

[10]Blasco, R. and Moss, B. Extracellular vaccinia virus formation and cell-to-cell virus transmission are prevented by deletion of the gene encoding the 37,000-Dalton outer envelope protein.*Journal Virology.* 1991, 65: 5910-5920 http://dx.doi.org/10.1128/jvi.65.11.5910-5920.1991.

[11]Schmutz, C., *et al.* A mutation in the gene encoding the vaccinia virus 37,000-M(r) protein confers resistance to an inhibitor of virus envelopment and release.*J Virol.* 1991, 65: 3435-42 http://dx.doi.org/10.1128/JVI.65.7.3435-3442.1991.

[12]Tan, C., *et al.* Development of multi-epitope vaccines against the monkeypox virus based on envelope proteins using immunoinformatics approaches.*Front Immunol.* 2023, 14: 1112816 http://dx.doi.org/10.3389/fimmu.2023.1112816.

[13]Lorenzo, M.M., *et al.* Mutagenesis of the palmitoylation site in vaccinia virus envelope glycoprotein B5.*J Gen Virol.* 2012, 93: 733-743 http://dx.doi.org/10.1099/vir.0.039016-0.

[14]Perdiguero, B. and Blasco, R. Interaction between vaccinia virus extracellular virus envelope A33 and B5 glycoproteins.*J Virol.* 2006, 80: 8763-77 http://dx.doi.org/10.1128/JVI.00598-06.

[15]Isaacs, S.N., *et al.* Characterization of a vaccinia virus-encoded 42-kilodalton class I membrane glycoprotein component of the extracellular virus envelope.*J Virol.* 1992, 66: 7217-24 http://dx.doi.org/10.1128/JVI.66.12.7217-7224.1992.

[16]Engelstad, M. and Smith, G.L. The vaccinia virus 42-kDa envelope protein is required for the envelopment and egress of extracellular virus and for virus virulence.*Virology.* 1993, 194: 627-37 http://dx.doi.org/10.1006/viro.1993.1302.

[17]Honeychurch, K.M., *et al.* The vaccinia virus F13L YPPL motif is required for efficient release of extracellular enveloped virus.*J Virol.* 2007, 81: 7310-5 http://dx.doi.org/10.1128/JVI.00034-07.

[18]O'Neil, M.J., *et al.* Successful Distribution of Tecovirimat During the Peak of the Mpox Outbreak - Los Angeles County, June 2022-January 2023.*MMWR Morb Mortal Wkly Rep.* 2024, 73: 546-550 http://dx.doi.org/10.15585/mmwr.mm7324a2.

[19]Ali, Y., *et al.* Fragment-Based Approaches Identified Tecovirimat-Competitive Novel Drug Candidate for Targeting the F13 Protein of the Monkeypox Virus.*Viruses.* 2023, 15: http://dx.doi.org/10.3390/v15020570.

[20]Wang, J., *et al.* An Overview of Antivirals against Monkeypox Virus and Other Orthopoxviruses.*J Med Chem.* 2023, 66: 4468-4490 http://dx.doi.org/10.1021/acs.jmedchem.3c00069.

[21]DeLaurentis, C.E., *et al.* New Perspectives on Antimicrobial Agents: Tecovirimat for Treatment of Human Monkeypox Virus.*Antimicrob Agents Chemother.* 2022, 66: e0122622 http://dx.doi.org/10.1128/aac.01226-22.

[22]Frenois-Veyrat, G., *et al.* Tecovirimat is effective against human monkeypox virus in vitro at nanomolar concentrations.*Nat Microbiol.* 2022, 7: 1951-1955 http://dx.doi.org/10.1038/s41564-022-01269-8.

[23]Duraffour, S., *et al.* Specific targeting of the F13L protein by ST-246 affects orthopoxvirus production differently.*Antivir Ther.* 2008, 13: 977-90 http://www.ncbi.nlm.nih.gov/pubmed/19195323.

[24]Geada, M.M., *et al.* Movements of vaccinia virus intracellular enveloped virions with GFP tagged to the F13L envelope protein.*J Gen Virol.* 2001, 82: 2747-2760 http://dx.doi.org/10.1099/0022-1317-82-11-2747.

[25]Lam, H.Y.I., *et al.* In Silico Repurposed Drugs against Monkeypox Virus.*Molecules.* 2022, 27: http://dx.doi.org/10.3390/molecules27165277.

[26]Duraffour, S., *et al.* ST-246 is a key antiviral to inhibit the viral F13L phospholipase, one of the essential proteins for orthopoxvirus wrapping.*J Antimicrob Chemother.* 2015, 70: 1367-80 http://dx.doi.org/10.1093/jac/dku545.

[27]Li, D., *et al.* Targeting F13 from monkeypox virus and variola virus by tecovirimat: Molecular simulation analysis.*J Infect.* 2022, 85: e99-e101 http://dx.doi.org/10.1016/j.jinf.2022.07.001.

[28]Bojkova, D., *et al.* Drug Sensitivity of Currently Circulating Mpox Viruses.*N Engl J Med.* 2023, 388: 279-281 http://dx.doi.org/10.1056/NEJMc2212136.

[29]Garrigues, J.M., *et al.* Identification of Tecovirimat Resistance-Associated Mutations in Human Monkeypox Virus - Los Angeles County.*Antimicrob Agents Chemother.* 2023, 67: e0056823 http://dx.doi.org/10.1128/aac.00568-23.

[30]Smith, T.G., *et al.* Tecovirimat Resistance in Mpox Patients, United States, 2022-2023.*Emerg Infect Dis.* 2023, 29: 2426-2432 http://dx.doi.org/10.3201/eid2912.231146.

[31]Mitja, O., *et al.* Mpox in people with advanced HIV infection: a global case series.*Lancet.* 2023, 401: 939-949 http://dx.doi.org/10.1016/S0140-6736(23)00273-8.

[32]Garcia, E.A., *et al.* Severe Mpox Among People With Advanced Human Immunodeficiency Virus Receiving Prolonged Tecovirimat in New York City.*Open Forum Infect Dis.* 2024, 11: ofae294 http://dx.doi.org/10.1093/ofid/ofae294.

[33]Hwang, J.H. and Hwang, J.H. Is a 2-week regimen of tecovirimat sufficient for the treatment of Mpox (monkeypox) in advanced HIV patients with a low CD4 cell count?*J Med Virol.* 2024, 96: e29617 http://dx.doi.org/10.1002/jmv.29617.

[34]Bourner, J., *et al.* Expanded Access Programme for the use of tecovirimat for the treatment of monkeypox infection: A study protocol for an Expanded Access Programme.*PLoS One.* 2024, 19: e0278957 http://dx.doi.org/10.1371/journal.pone.0278957.

[35]Harrison, I., *et al.* Brincidofovir for disease progression due to suspected tecovirimat resistance in association with advanced HIV.*Int J STD AIDS.* 2024, 35: 651-653 http://dx.doi.org/10.1177/09564624241238813.

[36]Karan, A., *et al.* Surveillance of Complicated Mpox Cases Unresponsive to Oral Tecovirimat in Los Angeles County, 2022.*J Infect Dis.* 2024, 229: S249-S254 http://dx.doi.org/10.1093/infdis/jiad517.

[37]Kato, N., *et al.* Inhibition of release of vaccinia virus by N1-isonicotinoly-N2-3-methyl-4-chlorobenzoylhydrazine.*J Exp Med.* 1969, 129: 795-808 http://dx.doi.org/10.1084/jem.129.4.795.

[38]Coll, J.M. Evolutionary-docking targeting bacterial FtsZ.*ChemRxiv.* 2023, https://chemrxiv.org/engage/chemrxiv/article-details/6405c36fcc600523a3bcb679: http://dx.doi.org/10.26434/chemrxiv-2023-ld9d3

[39]Wahl, J., *et al.* Accuracy evaluation and addition of improved dihedral parameters for the MMFF94s.*J Cheminform.* 2019, 11: 53 http://dx.doi.org/10.1186/s13321-019-0371-6.

[40]Coll, J. Could Acinetobacter baumannii LoI-abaucin docking be improved?*ChemRxiv.* 2023, https://chemrxiv.org/engage/chemrxiv/article-details/649aa71aba3e99daef1d1756: http://dx.doi.org/10.26434/chemrxiv-2023-962ht.

[41]Bryant, P., *et al.* Structure prediction of protein-ligand complexes from seqeunce information with Umol.*bioRxiv.* 2023: http://dx.doi.org/10.1101/2023.11.03.565471.

[42]Coll, J. Star-shaped Triazine-derivatives: would they crossbind SARS-CoV-2 spike helices?*ChemRxiv.* 2021, https://chemrxiv.org/engage/chemrxiv/article-details/6133c1096563696d9d222bbd: http://dx.doi.org/10.33774/chemrxiv-2021-xb6sx-v2.

[43]Lorenzo, M.M., *et al.* Would it be possible to stabilize prefusion SARS-COV-2 spikes with ligands?*ChemRxiv.* 2021: http://dx.doi.org/10.26434/chemrxiv.13453919.v2.

[44]Bermejo-Nogales, A., *et al.* Computational ligands to VKORC1s and CYPs. Could they predict new anticoagulant rodenticides?*BioRxiv.* 2021: http://dx.doi.org/10.1101/2021.01.22.426921.

[45]Dallakyan, S. and Olson, A.J. Small-molecule library screening by docking with PyRx.*Methods Mol Biol.* 2015, 1263: 243-50 http://dx.doi.org/10.1007/978-1-4939-2269-7_19.

[46]Morris, G.M., *et al.* AutoDock4 and AutoDockTools4: Automated docking with selective receptor flexibility.*J Comput Chem.* 2009, 30: 2785-91 http://dx.doi.org/10.1002/jcc.21256.

[47]Huey, R., *et al.* A semiempirical free energy force field with charge-based desolvation.*J Comput Chem.* 2007, 28: 1145-52 http://dx.doi.org/10.1002/jcc.20634.

[48]Trott, O. and Olson, A.J. AutoDock Vina: improving the speed and accuracy of docking with a new scoring function, efficient optimization, and multithreading.*J Comput Chem.* 2010, 31: 455-61 http://dx.doi.org/10.1002/jcc.21334.

[49]Lee, M., *et al.* Prolonged viral shedding in an immunocompromised Korean patient infected with hMPXV, sub-lineage B.1.3, with acquired drug resistant mutations during tecovirimat treatment.*J Med Virol.* 2024, 96: e29536 http://dx.doi.org/10.1002/jmv.29536.

[50]Shin, S.U., *et al.* Case report: atypical presentation of mpox with massive hematochezia and prolonged viral shedding despite tecovirimat treatment.*BMC Infect Dis.* 2024, 24: 183 http://dx.doi.org/10.1186/s12879-024-09098-2.

[51]Yang, G., *et al.* An orally bioavailable antipoxvirus compound (ST-246) inhibits extracellular virus formation and protects mice from lethal orthopoxvirus Challenge.*J Virol.* 2005, 79: 13139-49 http://dx.doi.org/10.1128/JVI.79.20.13139-13149.2005.

[52]Ferruz, N., *et al.* ProtGPT2 is a deep unsupervised language model for protein design.*Nat Commun.* 2022, 13: 4348 http://dx.doi.org/10.1038/s41467-022-32007-7.

[53]Ferruz, N. and Hocker, B. Dreaming ideal protein structures.*Nat Biotechnol.* 2022, 40: 171-172 http://dx.doi.org/10.1038/s41587-021-01196-9.

[54]Ferruz, N., *et al.* From sequence to function through structure: Deep learning for protein design.*Comput Struct Biotechnol J.* 2023, 21: 238-250 http://dx.doi.org/10.1016/j.csbj.2022.11.014.

[55]Grechishnikova, D. Transformer neural network for protein-specific de novo drug generation as a machine translation problem.*Sci Rep.* 2021, 11: 321 http://dx.doi.org/10.1038/s41598-020-79682-4.

[56]Ivanenkov, Y.A., *et al.* Chemistry42: An AI-Driven Platform for Molecular Design and Optimization.*J Chem Inf Model.* 2023, 63: 695-701 http://dx.doi.org/10.1021/acs.jcim.2c01191.

[57]Kang, K.M., *et al.* AI-based prediction of new binding site and virtual screening for the discovery of novel P2X3 receptor antagonists.*Eur J Med Chem.* 2022, 240: 114556 http://dx.doi.org/10.1016/j.ejmech.2022.114556.

[58]Mock, M., *et al.* AI can help to speed up drug discovery - but only if we give it the right data.*Nature.* 2023, 621: 467-470 http://dx.doi.org/10.1038/d41586-023-02896-9.

[59]Tsaban, T., *et al.* Harnessing protein folding neural networks for peptide-protein docking.*Nat Commun.* 2022, 13: 176 http://dx.doi.org/10.1038/s41467-021-27838-9.